NANO LETTERS

pubs.acs.org/NanoLett

Two-Photon-Coincidence Fluorescence Spectra of Cavity Multipolaritons: Novel Signatures of Multiexciton Generation

Oleksiy Roslyak,*,† Godfrey Gumbs,† and Shaul Mukamel‡

†Physics and Astronomy Department, Hunter College, CUNY, New York 10065 and ‡Chemistry Department, University of California, Irvine, California 92697-2025

ABSTRACT In a simulation study, we show that correlated two-dimensional frequency-resolved fluorescence spectra of a quantum dot in a microcavity provide a sensitive probe for the distribution of multiexcitons. Polariton couplings lead to a fine structure of Rabi multiplets that allow us to resolve otherwise overlapping features of the different multiexcitons. These may be used to probe multiexciton generation.

KEYWORDS Carrier multiplication, multiexcitons, biexciton, 2D spectroscopy, nanocrystal quantum dots

Multiexciton generation (MEG)[1−3] in quantum dots (QDs) produces multiple electron−hole pairs (multiexcitons) upon absorption of a single photon and can thus enhance the efficiency of solar cells. In a typical transient absorption (TA) or fluorescence (TF) experiment, a pump photon of energy well above the excitonic band gap, for example, $\hbar\omega = 3E_g$, creates high energy carriers whose inelastic scattering generates the multiexcitons. In bulk semiconductors, competition from ultrafast interband relaxation due to electron−phonon scattering and momentum conservation in the crystal result in a low MEG efficiency and high activation energy for their formation.[4,5] In QDs some of these processes may be suppressed or enhanced due to the discrete energy level structure and since momentum conservation no longer holds. The "phonon bottleneck" effect reduces phonon-assisted relaxation rates. On the other hand increased electron-hole Coulomb interaction greatly enhances the rate of Auger cooling as well as the inverse Auger process of impact ionization. The former is the process whereby the hot electron relaxes to its ground state and the excess energy is transferred via Coulomb scattering to the hole, which is excited deep into the valence band. The latter describes a highly excited carrier decaying to its ground state meanwhile exciting a valence electron across the band gap, thus producing two electron-hole pairs from one. Numerous experiments suggest that this is the primary mechanism for MEG QD's (see refs 6 and 7 and references therein). TA measurements focus on the pump-induced absorption changes of the probe that are primarily attributed to the Coulomb interactions.[4,8] MEG is usually followed by Auger recombination of multiexcitons. The MEG quantum yield (QY) is defined as the number of electron−hole pairs harvested from a pump photon of a given energy. The MEG-induced changes in TA had suggested that a single photon could generate up to seven e−h pairs (QY = 7) in PbSe[1,6] after a certain energy threshold the QY becomes linear with the pump photon energy. Environment and growth methods of QD's may reduce the QY. In contrast, some recent TF spectroscopy experiments performed on CdSe and CdTe nanocrystals showed no MEG.[9] TF is particularly sensitive to the relaxation mechanisms that compete with radiative recombination. Both types of the transient signals are based on the deviation of the multiexciton distribution from the Poissonic form expected for TF induced by multiphoton absorption without MEG.[1,10] An alternative MEG model, based on the exciton spectral density, was proposed in ref 11. A more detailed description of MEG dynamics based on series of odd-ordered interband scattering events was developed in ref 7. In all transient measurements, the multiexciton states are distinguished by their different Auger rates. However this analysis is not always straightforward since the Auger process may be suppressed if the multiexcitons are redistributed among several QD via, for instance the Forster mechanism. In ref 12, the authors argue that resonant Forster transfer can be as fast or faster than Auger process once the QD's are embedded in organic layers. In fact, it competes with the impact ionization which is all but instantaneous (<200 fs in some cases). Because of this competition, it was hard to pinpoint the carrier multiplication using conventional transient techniques which are based on monitoring discrete Auger decay. Such transfer is beyond the scope of the presented theory, but one could easily replace the polariton picture with the hybrid organic/QD exciton in search for the MEG effect in the photoluminescence spectra. Of course, the nonlinearities acquired in the organic material may play crucial role.) Developing new spectroscopic probes for the distribution of number of

* To whom correspondence should be addressed. E-mail: avroslyak@gmail.com.
Received for review: 06/15/2010
Published on Web: 09/30/2010

DOI: 10.1021/nl1020969 | *Nano Lett.* **2010,** *10,* 4253–4259

multiexcitons could help pinpoint the MEG mechanism. Frequency-resolved fluorescence is not adequate since the various transitions between N and $N-1$ exciton states overlap.

In this letter, we argue that these difficulties may be overcome by inserting the QD in a resonant microcavity. The excitons then become dressed with photons thus forming elementary excitations known as polaritons. The entanglement between excitons and photons results in a fine structure of the multipolariton states. When the excitons may be treated as weakly interacting bosons, this fine structure is represented by Rabi multiplets in the emission spectra. Unlike multiexciton emission, the Rabi multiplets may be well separated spectrally and may reveal the initial polariton distribution. Here, we show that the frequency resolved single and two-photon fluorescence correlation spectra are highly sensitive to the number of excitons and may thus be utilized as a probe for the MEG mechanism.

A QD in a microcavity is described by the Hamiltonian[13−15]

$$\begin{aligned} H &= H_{\mathrm{sys}} + H_{\mathrm{int}} \\ H_{\mathrm{sys}} &= \hbar\omega_{1S}B^{\dagger}B + \hbar g B^{\dagger}B^{\dagger}BB + \hbar\omega_{C}a^{\dagger}a + \\ &\qquad \hbar G(a^{\dagger}B + B^{\dagger}a) \\ H_{\mathrm{int}} &= -\mu_{1S}\sum_{i}(E_{i}B^{\dagger} + E_{i}^{\dagger}B) \end{aligned} \tag{1}$$

The first two terms in H_{sys} represent a weakly interacting boson model. The first term defines the lowest energy $\hbar\omega_{1S}$ QD excitons by means of its creation operator $B^{\dagger} = b^{\dagger} - \nu b^{\dagger}b^{\dagger}b$, where b are boson operators with $[b, b^{\dagger}] = 1$ and ν is the phase-filling parameter. The second term, $\sim g$, is responsible for Coulomb exciton−exciton scattering. The parameters g and ν may be adjusted to represent the exciton energies and transition dipoles of the QD. These parameters can adequately represent the system with a few excitons as follows from either Usui transformation[16] or the renormalized bosonic interaction of excitons.[13] Alternatively, g can be extracted from the MEG activation energy threshold as argued by Schaller in ref 17. This gives $g \sim 2-9$ meV in the core−shell configuration of the QDs. In refs 18 and 19, a "giant" exciton−exciton repulsion of 100 meV is reported, and tools to calculate/measure (transient absorption/bleaching) this quantity are provided. For typical QDs one has $g/\nu G = 3$,[20] unless one filters out the left (or right) circular polarization of the cavity photons,[13] making the ratio to be $g/\nu G \ll 1$. Additional terms in the expansion of $B^{\dagger}$ and the Hamiltonian may be needed for a more accurate description of the multiexcitonic states.[21] By treating these parameters phenomenologically, we can describe a broad range of type and shape of QDs.

The third and the fourth terms in H_{sys} describe the microcavity and its coupling to the QD, respectively. We assume a single cavity mode with frequency ω_C and creation (annihilation) operators $a^{\dagger}(a)$; G is the Rabi frequency. H_{int} represents the interaction of the QD with the continuum of free-field mode i with the electric field operator $E_i(t) + E_i^{\dagger}(t)$. If we expand H_{sys} in $b^{\dagger}(b)$ to quadratic order, we can diagonalize it using Schwinger's angular momentum representation of bosonic operators.[22,20] We can then treat the higher order terms perturbatively to first order in g and ν, thus obtaining the polariton energies $E_{j,m}$ and transition dipole moments $\mu_{j\,m;\,j',m'}$ (see Supporting Information for details). For a fixed number N of polaritons, $j = N/2$ describes polariton levels and $m = N/2, \ldots, -N/2$ stands for the sublevels (polariton fine structure). This representation gives $j+m$ photons in the microcavity and $j-m$ excitons in the QD. Simple algebra based on Baker-Hausdorff identity[22] yields intralevel transitions selection rule $\Delta j = -1/2$ for spontaneous emission into the free field mode. The sublevels selection rules are more complicated and depend on the Coulomb and phase-filling nonlinearities. For the quadratic polariton Hamiltonian, we have $\Delta m = \pm 1$. These selection rules are relaxed by higher order terms in the Hamiltonian thus allowing $\Delta m = \pm 3/2, \pm 5/2$. The model Hamiltonian takes into account only one type of excitons. The lowest 1S with the energy approximately given by the semiconductor gap $\hbar\omega_{1S} \approx E_g$. Thus, this model is suitable only for photoluminescence. Photon absorption and, more importantly, the details of multiexciton formation (ether by direct photogeneration or impact ionization) lie beyond such description. A general formalism and framework that accounts for various types of excitons and biexcitons was developed in ref 23 see also references therein. There are several advantages to our simplified model over the first-principle calculations. These include description of polariton states formed by multiexcitons of higher order than biexcitons and fully analytical expressions for the fluorescence signals. These will be calculated using the polariton eigenvalues, transition dipoles, and dephasing rates (see Supporting Information for details). The frequency-resolved fluorescence is described by the Close time path loop (CTPL) diagram shown in Figure 1a[24,25] yielding

$$S^{(1)}(\omega_1) \sim \mathrm{Im}\sum_{j}\sum_{m=-j}^{j}\sum_{m1=-j+1/2}^{j-1/2} P(j,m)\left|\mu_{j,m;j-1/2,m1}\right|^2 \times G^{*}_{j,m;j0-1/2,m1}(\omega_1) \tag{2}$$

Here $P(j, m)$ is the distribution of states; Green's functions are the matrix elements of the propagator in the polariton basis $G_{j,\,m;\,j-1/2,\,m1}(\omega) = \hbar(\hbar\omega - (E_{j,\,m} - E_{j-1/2,\,m1}) + \hbar\gamma)^{-1}$; the dephasing rate of the corresponding transition γ is related to the quality factor of the cavity by $Q = \omega_C/\gamma$.

A higher level observable is the two-photon correlation spectrum obtained by detecting both ω_1 and ω_2 photons within a gated time window. The corresponding CTPL shown in Figure 1b gives

DOI: 10.1021/nl1020969 | Nano Lett. 2010, 10, 4253–4259

$$S^{(3)}(\omega_1,\omega_2) \sim -\mathrm{Im}\sum_j \sum_{m=-j}^{j} P(j,m) \times \sum_{m1=-j+1/2}^{j-1/2} \sum_{m2=-j+1}^{j-1} |\mu^*_{j,m;j-1/2,1}\mu^*_{j-1/2,m1;j-1,m2}|^2 \times G^*_{j,m;j-1,m2}(\omega_1+\omega_2)|G_{j,m;j-1/2,m1}(\omega_1)+G_{j,m;j-1/2,m1}(\omega_2)|^2 \quad (3)$$

When the pump beam is off-resonance, the system finds itself in a mixed multipolariton state. Both $S^{(1)}$ and $S^{(3)}$ depend on population distribution $P(j, m)$, which determines the specifics of the population mechanism and can be utilized to search for MEG. Since the polariton sublevels m are very close in energy as compared to levels j separation, we shall assume that the initial distribution of the polaritons is independent of the sublevel index and set $P(j, m) \rightarrow P(j)$. We then use the phenomenological theory developed in refs 1 and 10 to calculate polariton population distribution.

Let us first ignore MEG and consider multiphoton-induced fluorescence. When the pump photon energy is much larger than energy gap E_g, carrier-induced absorption saturation is negligible. Thus, the probability of generation of an electron/hole pair is independent of the number of pairs already existing. This yields a Poisson probability distribution to have N polaritons in a QD

$$P(j,\langle N_0\rangle) = \frac{\langle \tilde{N}_0\rangle^{2j}}{2j}\frac{\exp(-\langle \tilde{N}_0\rangle}{(2j)!} \quad (4)$$

$$\langle \tilde{N}_0\rangle = \langle N_0\rangle\left(1 - \frac{1}{2}\langle N_0\rangle v\right) \quad (5)$$

The average single exciton population, $\langle N_0\rangle$, is an experimentally determined parameter proportional to the pump fluence j_p as $\langle N_0\rangle = j_p\sigma_a$ with σ_a being the QD absorption

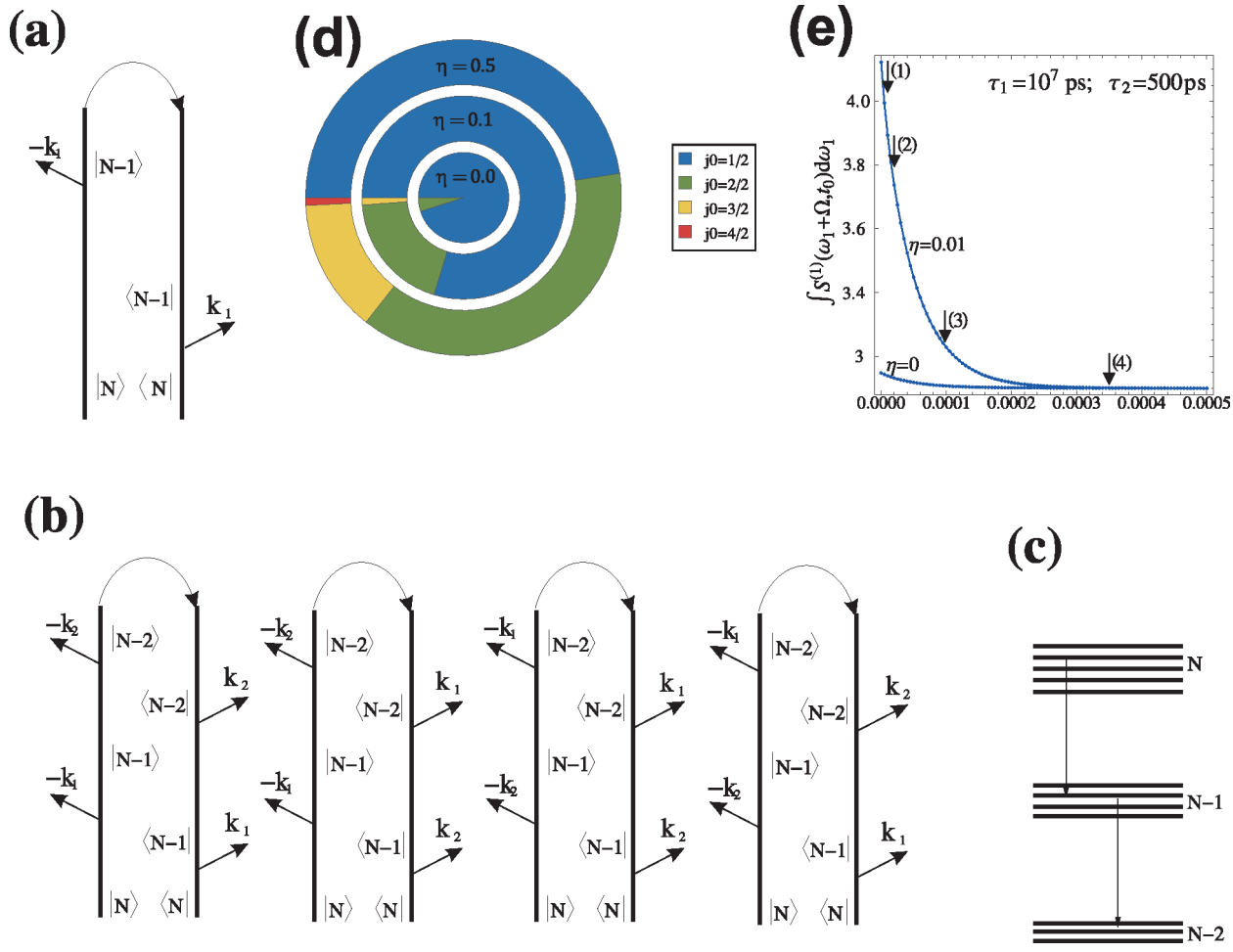

FIGURE 1. Closed time path loop diagrams for (a) one-photon and (b) two-photon fluorescence. (c) Level scheme of polaritons. The arrows indicate transitions between j^{th} levels (sublevels selection rules are not shown). (d) Relative contribution of the multipolariton states to the fluorescence signal for various values of the MEG defining phenomenological parameter η. (e) Time-resolved frequency-integrated single photon fluorescence at various delays (1−4) from the pump. These may be used to assign the multiexciton transitions in the correlation spectra for large exciton nonlinearities g, v.

DOI: 10.1021/nl1020969 | Nano Lett. 2010, 10, 4253–4259

cross-section. Equation 5 accounts for the nonbosonic nature of the excitons.[26]

The MEG mechanism produces non-Poison distributions. We shall use the following model MEG-induced polariton distribution[10] for pump energy in the range $3E_g < \hbar\omega_p < 4E_g$

$$P(j,\langle N_0\rangle,\eta) = \sum_{n'=\lceil 2j/3\rceil}^{2j-1} P(n',\langle N_0\rangle) \sum_{n=2j-1}^{2n'} \eta^n(1-\eta)^{2n'-n}\frac{(2n')!}{n!(2n'-n)!} \quad (6)$$

The parameter η is related to the quantum yield by $\eta = (QY - 1)/2$; the integer $[2j/3]$ means the ceiling of the ratio. For $\eta = 0$, this reduces to the Poison distribution as in eq 4. Relative multipolariton contributions for various η are depicted in Figure 1d. Note that $P(j, m)$ could be alternatively calculated by using the spectral density of the multiexciton states, as proposed in ref 11. In that model, the quantum yield is the average exciton multiplicity. However this would require many adjustable parameters related to the underlying relaxation mechanism.

We assume the following microcavity parameters: the cavity mode is resonant with the exciton $\omega_c = \omega_{1S} \equiv \Omega$. (The microcavity is made either of Bragg stacked mirrors[27] or a photonic crystal nanocavity.[28,29]) We display the signals vs. the detuning between the emitted light and the central frequency $\omega_1 - \Omega$. Assuming a quality factor, $Q = 13\,000$ gives the dephasing rate $\gamma = 0.01$ meV. (Typical QD exciton lifetime is 10^{-7} s and the biexciton lifetime is 500 ps, thus their contribution to γ can be neglected.) The quantum dot is assumed to be able to accommodate at least four excitons in the 1S lowest state. This will allow us to neglect possible saturation effects and the signatures of multiexcitons formed by various types of excitons. Lead salts (PbS, PbSe, and PbTe) quantum dots[30] of radius more than 10 nm are good candidates for our model. These have direct band gaps (for PbSe, $E_g = 0.28$ eV) at four equivalent L points in the Brillouin zone. The bottom of the conduction band has L_6^- symmetry in the double group notation, and the top of the valence band has L_6^+ symmetry.[31] Spatially, the valence band-edge Bloch functions are s-like, while the conduction band-edge Bloch functions are $p_{\langle 111\rangle}$-like, where $\langle 111\rangle$ denotes the direction in the cubic lattice. Therefore the transitions are optically active and may be described by the transition dipole moment μ_{cv}. On average, only one percent of the quantum dots absorbs more than one photon $\langle N_0\rangle = 0.01$. We are thus far from saturation. This parameter defines the Poisson distribution eq 4 and the multiphoton induced fluorescence. To describe MEG-induced fluorescence, we vary the parameter $\eta > 0$.

Figure 2 displays the fluorescence spectra in the strong polariton coupling regime $G \gg g \gg \nu G$. The following QD parameters were used: exciton-microcavity central mode coupling $G = 2.5$ meV, the Coulomb matrix element $g = 0.3$ meV (so that $G \gg g$), and the phase filling is neglected $\nu = 0$. In the absence of MEG ($\eta = 0$, QY = 1) we have standard polariton emission. There are two resonances (Rabi doublet) provided by single polariton state and separated by $2G$ as shown in Figure 2(1.1). The contributions of multipolariton states emission are too weak to be observable in $S^{(1)}$. However they are clearly seen in the correlation spectra depicted in Figure 2(1.2). The correlation resonances occur between ω_1 photon and virtual double photon $\omega_1 + \omega_2$. In accordance with eq 3, the ω_1 resonances occur at the poles of the retarded Green's function $G_{j0,\,m0;\,j0-1/2,\,m1}(\omega_1)$ while the virtual double photon $\omega_1 + \omega_2$ resonances are given by the poles of the advanced Green's function across the loop $G^*_{j0,\,m0;\,j0-1,\,m2}(\omega_1 + \omega_2)$. More precisely the correlation between $N = 1$ (horizontal axes) and $N = 2$ (vertical axes) show a ladder-like pattern resonances with horizontal and vertical steps the size of G and $2G$ respectively. We shall refer to these resonances as group A. For stronger MEG with $\eta = 0.1$ (QY = 1.2) the multipolariton emission is enhanced. Two additional peaks from $N = 2$ manifold and separated by $4G$ are seen in Figure 2(2.1). They correspond to Rabi quadruplet. The central two peaks are masked by the Rabi doublet. The $S^{(3)}$ spectra (Figure 2(2.2)) also reveal correlation between $N = 3$ and $N = 2$ manifolds (group B). Further increase of the quantum yield ($\eta = 0.5$, QY = 2) shows $N = 3$ Rabi multiplet (Figure 2(3.1)). The central peaks of which are masked by the lower multiplets. Correlation resonances between $N = 3$ and $N = 4$ polariton states appears in Figure 2(3.2). Rabi multiplets are slightly split by the Coulomb interaction.

Figure 3 depicts spectra for QD with $G = g = 2.5$ meV and $\nu = 1/3$. Because of strong nonlinearities, multipolariton transitions are seen even in absence of the MEG. However they become more pronounced with MEG. The Rabi multiplets become asymmetric and the emission is predominantly given by the excitonic part of the polariton manifolds. The Coulomb splitting is strong enough to mix the resonances from various multiplets. To assign the resonances and correlation resonances, we can record the spectra at different time snapshots after the pump. Different polaritons have different lifetimes τ_{j0} that follow from the biexciton τ_1 lifetime[32] as $\tau_{j0} = \tau_1/j0^2$. These describe Auger decay of the polaritons via its excitonic part. We take snapshots at various t_0 's along the Auger driven multiexciton relaxation as shown in the frequency integrated spectra (Figure 1e). Because of quantized Auger lifetimes the contributions from the multipolariton manifolds become less pronounced sequentially. The contributions from $N = 4$ relax first then $N = 3$ and so on until we are left with the Rabi doublet ($N = 2$).

One of the most striking results of our simulations is that the fluorescence spectra from the pure excitons ($G \to 0$) are not sensitive to the MEG parameter η. This holds for all confinement regimes above the saturation limit. Using near degenerate perturbation theory we obtain that with and

DOI: 10.1021/nl1020969 | Nano Lett. 2010, 10, 4253–4259

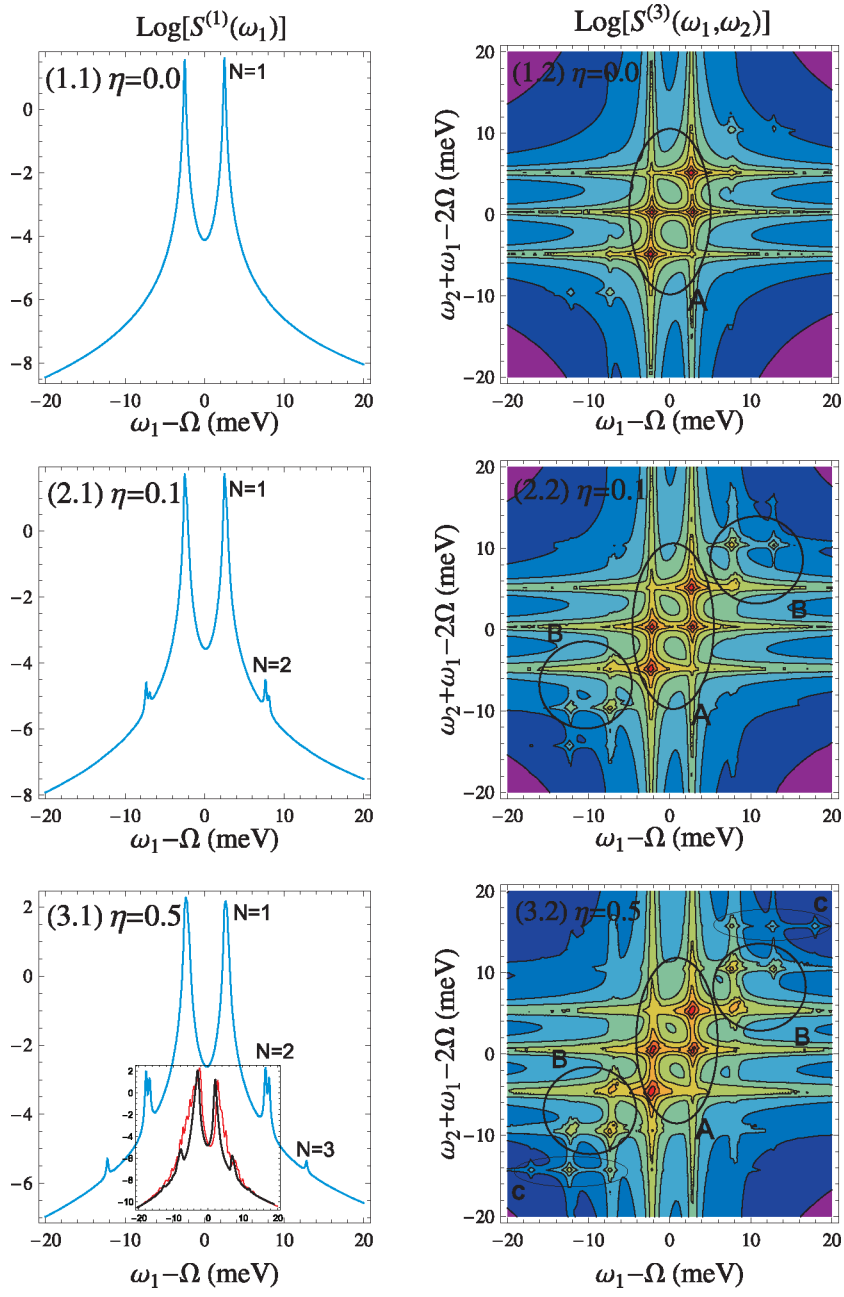

FIGURE 2. Multipolariton single-photon (left panels) and two-photon (right panels) fluorescence spectra for small exciton nonlinearities with ($\eta > 0$) and without ($\eta = 0$) MEG. Region (C) shows correlation resonances (CR) between $N = 4$ and $N = 3$ levels. Region (B) also includes CR from $N = 3$ and $N = 2$ levels. Region (A) includes, in addition to the above, CR from $N = 2$ and $N = 1$ levels. Insets show inhomogeneous broadening of the signal with $\sigma_{1S} = G$ (black) and $\sigma_{1S} = 2G$ (red).

without MEG the central exciton resonance is just split into multiple exciton resonances separated by g (See Figure 3(3.1),(3.2)). For excitons $\nu G \rightarrow 0$ phase space filling only modifies the relative peak intensities. Given the large dephasing rate these multiexciton resonances result in a non-Lorentzian line shape.[33] Analogously, the polariton spectra become insensitive to the MEG mechanism for increasing detuning $\Delta = \omega_C - \omega_{1S}$. For moderate detuning, the relative intensity (but not the frequencies)) of the multiexcitonic peaks of the polariton emission is still sensitive to MEG, but for large detuning that effect vanishes. On the other hand the polariton emission spectra are more sensitive to the MEG parameter η as the coupling G is increased. A notable advantage of the proposed technique is its ability to detect signatures of MEG for pump fluence an order of magnitude smaller than those required for conventional TF. This may be used for MEG detection in solar cells exposed to relatively low intensity sunlight.

As a concluding remark let us investigate the effect of ensemble averaging on MEG. We modeled the exciton

DOI: 10.1021/nl1020969 | *Nano Lett.* **2010,** *10,* 4253–4259

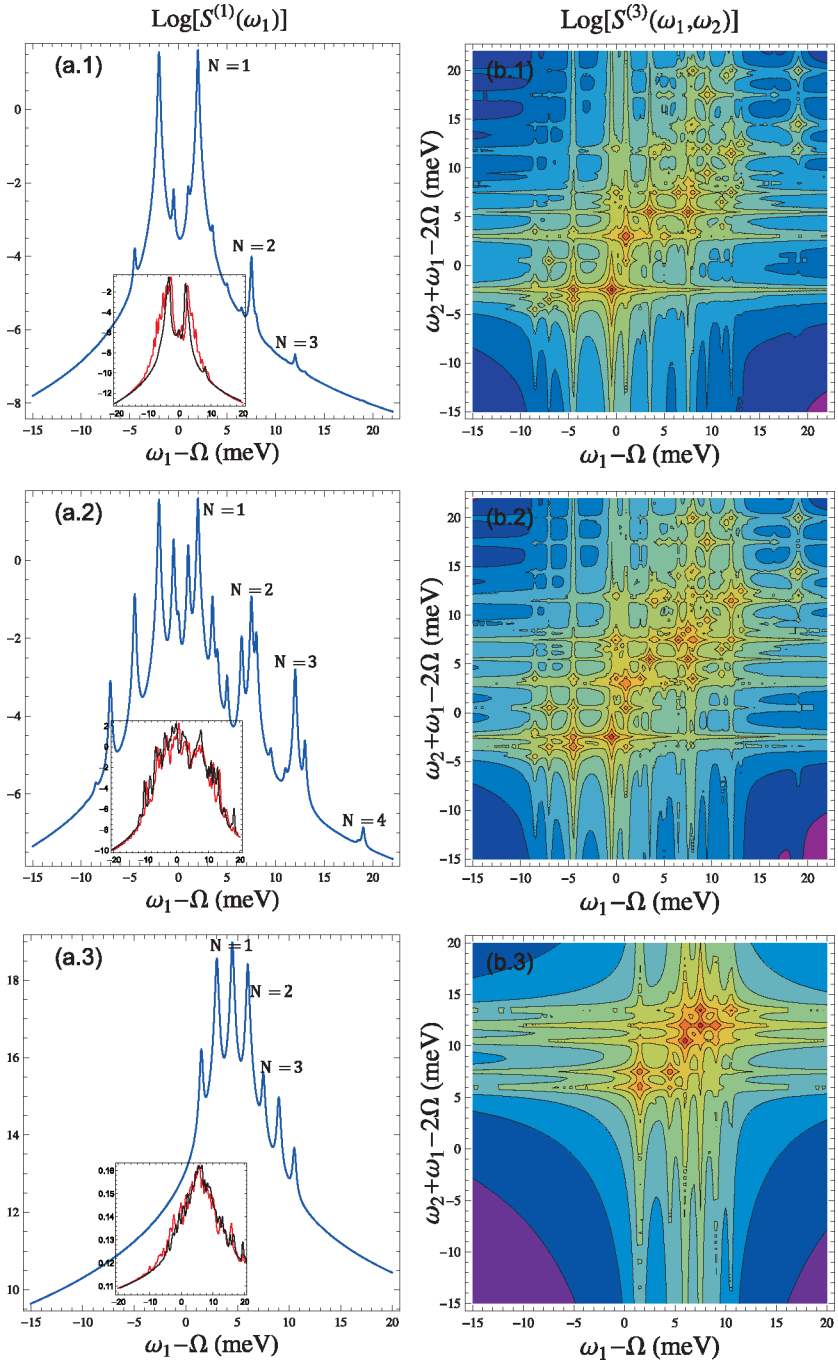

FIGURE 3. Single-photon (left (a)) and two-photon (right panels (b)) fluorescence spectra for exciton nonlinearities comparable to the exciton-photon coupling. Panels (1) and (2) show polariton fluorescence with ($\eta = 0.01$) and without ($\eta = 0$) MEG. Panels (3) show fluorescence with MEG from excitons in the absence of the micro cavity coupling ($G \rightarrow 0$). MEG does not affect these spectra. The resonances were assigned taking spectral snapshots along the Auger driven relaxation. Insets show inhomogeneous broadening of the signal with $\sigma_{1S} = g$ (black) and $\sigma_{1S} = 2g$ (red).

energy $\hbar\omega_{1S}$ as a Gaussian around the microcavity central frequency ω_c, with variance σ_{1S}. Such distribution, rather than more conventional QD size variation, is not limited to spherical QD's and avoids the introduction of some additional phenomenological parameters such as size dependent exciton energy shift.[34] This simplification is possible only because variation of the exciton energy on a scale of a few meV shall not produce any perceptible variation in g. Indeed, the variation of $g = 3-9$ meV mentioned before for the core−shell configuration required the variation in $\tilde{\omega}_{1S} = 0.85-1.05$ eV. We found that the distinct blue-shift of the central exciton resonance (of the order of g) is not affected by a few meV variation of the exciton energy. However the fine structure of exciton fluorescence spectra (Figure 3(d.1))

DOI: 10.1021/nl1020969 | *Nano Lett.* **2010,** *10,* 4253–4259

is bleached for σ_{s1} as small as $g/10$. This makes the exciton spectra not only insensitive to the quantum yield, but also impractical for extracting information about the multiexciton states. The spectral signatures of MEG of polaritons persist until the mean variance $\sigma_{1S} < G/\hbar$ (see insets in Figure 2). Some weak features due to Coulomb term become bleached out, but the peaks for $N = 2$, $N = 3$ become recognizable when QY reaches certain threshold value. For $\hbar\sigma_{1S} = \hbar G = 2.5$ meV, we found the threshold to be $\eta \approx 0.3$. For larger inhomogeneous broadening of the exciton energy the spectra bears the signatures of the single excitons coupled to the microcavity (see insets in Figure 2). This suggests that the preferable method would be to vertically resolve the spectra from different QDs.[35] In this case, one can neglect the inhomogeneous broadening and set spectral resolution to $\sim G/10$ meV. In the large nonlinearities regime, the MEG signatures persist up to a few g of the variance (see insets in Figure 3). Even though the fine structure is smeared the spectra are clearly distinct for various values of the quantum yield. For a given variance, the QY of the threshold for spectrally observing MEG of polaritons is substantially lowered by increasing exciton Coulomb scattering. It is surprising since usually it is a polaritons that are sensitive to the detuning. Their spectra are usually measured by varying the temperature, which slightly affects the exciton energy around the microcavity central frequency. In summary, the polariton spectra are sensitive to both the multiexciton distribution and exciton energy distribution. The first may allow to observe the multiexciton generation without referring to the transient measurement and discrete Auger lifetimes. On the other hand, the uncertainty in the QD size is an impeding factor for such measurements. For large Coulomb repulsion, one might observe the signatures of MEG of polaritons even from an ensemble of QDs with inhomogeneous broadening of the order of g.

Acknowledgment. This work was supported by Contract No. FA 9453-07-C-0207 of AFRL and the Air Force Office of Scientific Research (AFOSR). S.M. gratefully acknowledges the support of the Chemical Sciences, Geosciences, and Biosciences Division, Office of Basic Energy Sciences, Office of Science, U.S. Department of Energy.

Supporting Information Available. Additional calculations. This material is available free of charge via the Internet at http://pubs.acs.org.

REFERENCES AND NOTES

(1) Klimov, V. *Annu. Rev. Phys. Chem.* **2007**, *58*, 635.
(2) Nozik, A. *Inorg. Chem.* **2005**, *44*, 6893.
(3) McGuire, J.; Joo, J.; Pietryga, J.; Schaller, R.; Klimov, V. *Acc. Chem. Res.* **2008**, *41*, 1810.
(4) Klimov, V. *Appl. Phys. Lett.* **2006**, *89*, 123118.
(5) Harrison, D. *J. Appl. Phys.* **1999**, *85*, 8178.
(6) Nozik, A. *Chem. Phys. Lett.* **2008**, *457*, 3.
(7) Velizhanin, K.; Piryatinski, A.; Klimov, V. Effect of Photoexcitation and Population Relaxation on Carrier Multiplication Efficiency in Semiconductor Nanocrystals. APS Meeting Abstracts; 2010, arXiv: 0911.1139v.
(8) Klimov, V. Linear and Nonlinear Optical Spectroscopy of Semiconductor Nanocrystals. In *Handbook of Nanostructured Materials and Nanotechnology*; Nalwa, H. S.; Academic Press: San Diego, 2000.
(9) Ben-Lulu, M.; Mocatta, D.; Bonn, M.; Banin, U.; Ruhman, S. *Nano Lett.* **2008**, *8*, 1207.
(10) Beard, M.; Knutsen, K.; Yu, P.; Luther, J.; Song, Q.; Metzger, W.; Ellingson, R.; Nozik, A. *Nano Lett.* **2007**, *7*, 2506.
(11) Allan, G.; Delerue, C. *Phys. Rev. B* **2008**, *77*, 125340.
(12) Agranovich, V.; Czaijkowski, G. 2008, arXiv0801.3794.
(13) Inoue, J.-i.; Brandes, T.; Shimizu, A. *Phys. Rev. B* **2000**, *61*, 2863.
(14) Takagahara, T. *Phys. Rev. B* **1989**, *39*, 10206.
(15) Khitrova, G.; Gibbs, H.; Jahnke, F.; Kira, M.; Koch, S. *Rev. Mod. Phys.* **1999**, *71*, 1591.
(16) Hiroshima, T. *Phys. Rev. B* **1989**, *40*, 3862.
(17) Schaller, R.; Pietryga, J.; Klimov, V. *Nano Lett* **2007**, *7*, 3469–3476.
(18) Klimov, V.; Ivanov, S.; Nanda, J.; Achermann, M.; Bezel, I.; McGuire, J.; Piryatinski, A. *Nature* **2007**, *447*, 441–446.
(19) Piryatinski, A.; Ivanov, S.; Tretiak, S.; Klimov, V. *Nano Lett* **2007**, *7*, 108–115.
(20) Liu, Y.; Imoto, N.; "Ozdemir, Ş.; Jin, G.; Sun, C. *Phys. Rev. A* **2002**, *65*, 23805.
(21) Combescot, M.; Dupertuis, M. A. *Phys. Rev. B* **2008**, *78*, 235303.
(22) Beidenharn, L.; Louch, J. *Angular momentum in Quantum physics*; Addison-Wesley: London, 1981.
(23) Pirytinski, A.; Velizhanin, K. A. 2009, arXiv0911.1139.
(24) Marx, C.; Harbola, U.; Mukamel, S. *Phys. Rev. A* **2008**, *77*, No. 022110.
(25) Roslyak, O.; Mukamel, S. *Mol. Phys.* **2009**, *107*, 265.
(26) Avancini, S.; Krein, G. *J. Phys. A: Math. Gen.* **1995**, *28*, 685.
(27) Reithmaier, J.; Sek, G.; Loffler, A.; Hofmann, C.; Kuhn, S.; Reitzenstein, S.; Keldysh, L.; Kulakovskii, V.; Reinecke, T.; Forchel, A. *Nature* **2004**, *432*, 197.
(28) Wu, Z.; Mi, Z.; Bhattacharya, P.; Zhu, T.; Xu, J. *Appl. Phys. Lett.* **2007**, *90*, 171105.
(29) Yoshie, T.; Scherer, A.; Hendrickson, J.; Khitrova, G.; Gibbs, H.; Rupper, G.; Ell, C.; Shchekin, O.; Deppe, D. *Nature* **2004**, *432*, 200.
(30) Kang, I.; Wise, F. *J. Opt. Soc. Am. B* **1997**, *14*, 1632.
(31) Nimtz, G.; Schlicht, B. *Narrow-gap lead salts*; Springer-Verlag: Berlin, 1983.
(32) Klimov, V.; Mikhailovsky, A.; McBranch, D.; Leatherdale, C.; Bawendi, M. *Science* **2000**, *287*, 1011.
(33) Peterson, J.; Krauss, T. *Nano Lett* **2006**, *6*, 510–514.
(34) Micic, O. I.; Cheong, H. M.; Fu, H.; Zunger, A.; Sprague, J. R.; Mascarenhas, A.; Nozik, A. J. *J. Phys. Chem. B* **1997**, *101*, 4904–4912.
(35) Empedocles, S.; Neuhauser, R.; Shimizu, K.; Bawendi, M. *Adv. Mater.* **1999**, *11*, 1243–1256.

DOI: 10.1021/nl1020969 | *Nano Lett.* **2010,** *10,* 4253–4259